Evaluation of Surface and Near-Surface Melt Characteristics on the Greenland Ice Sheet using MODIS and QuikSCAT data

Dorothy K. Hall[1], Son V. Nghiem[2], Crystal B. Schaaf[3], Nicolo E. DiGirolamo[4]

and

Gregory Neumann[2]

[1]Cryospheric Sciences Branch, Code 614.1

NASA Goddard Space Flight Center

Greenbelt MD 20771

dorothy.k.hall@nasa.gov

[2]Jet Propulsion Laboratory, California Institute of Technology, Pasadena,

CA, 91109

[3]Department of Geography and Center for Remote Sensing, Boston University, Boston,

MA 02215

and

[4]Science Systems and Applications, Inc.

Lanham, MD 20706

Abstract

The Greenland Ice Sheet has been the focus of much attention recently because of increasing melt in response to regional climate warming. To improve our ability to measure surface melt, we use remote-sensing data products to study surface and near-surface melt characteristics of the Greenland Ice Sheet for the 2007 melt season when record melt extent and runoff occurred. Moderate Resolution Imaging Spectroradiometer (MODIS) daily land-surface temperature (LST), MODIS daily snow albedo, and a special diurnal melt product derived from QuikSCAT (QS) scatterometer data, are all effective in measuring the evolution of melt on the ice sheet. These daily products, produced from different parts of the electromagnetic spectrum, are sensitive to different geophysical features, though QS- and MODIS-derived melt generally show excellent correspondence when surface melt is present on the ice sheet. Values derived from the daily MODIS snow albedo product drop in response to melt, and change with apparent grain-size changes. For the 2007 melt season, the QS and MODIS LST products detect 862,769 km^2 and 766,184 km^2 of melt, respectively. The QS product detects about 11% greater melt extent than is detected by the MODIS LST product probably because QS is more sensitive to surface melt, and can detect subsurface melt. The consistency of the response of the different products demonstrates unequivocally that physically-meaningful melt/freeze boundaries can be detected. We have demonstrated that these products, used together, can improve the precision in mapping surface and near-surface melt extent on the Greenland Ice Sheet.

47 **Introduction**

48

49 Much of the Arctic has warmed in recent decades (Serreze et al., 2000), and remote
50 sensing technology has been instrumental in quantifying the attendant snow and ice
51 changes. Recently there has been a focus on the Greenland Ice Sheet because of its
52 importance to sea-level rise, and the observations of increasing Arctic surface
53 temperatures over the last few decades (Comiso, 2006; Wang and Key, 2005; Box, 2002),
54 and ice sheet mass loss over the last few years (e.g., Krabill et al., 2004; Luthcke et al.,
55 2006; Rignot et al., 2008). Melting of the entire Greenland Ice Sheet would contribute
56 approximately 7 m to sea level (Gregory et al., 2004). If the climate continues to warm at
57 the current rate, mass loss of the Greenland Ice Sheet will likely accelerate sea-level rise.
58 Field work and weather station data, especially from automatic-weather stations (AWS)
59 (Steffen and Box, 2001; van de Wal et al., 2006), have been useful for quantifying air and
60 surface-temperature changes, as have remotely-sensed data. It is vital to improve our
61 ability to monitor and predict the quantity of meltwater emanating from melting ice on
62 Greenland.

63

64

65 In this work, we blended three daily products derived from two different instruments: the
66 Moderate-Resolution Imaging Spectroradiometer (MODIS), and the SeaWinds
67 scatterometer on the QuikSCAT (QS) satellite. The products are: MODIS-derived
68 surface albedo, MODIS-derived surface temperature and QS-derived melt. MODIS
69 products are produced during clear-sky conditions only, while QS melt maps are obtained

during all sky conditions. We provide a quantitative comparison of daily melt derived from the various products and discuss the physical basis for melt detection. We also delineate surface and near-surface melt extent, detect incipient melt, and monitor the progression of melt. Results show the initiation, progression, extent and cessation of melt for the 2007 melt season which is known to have experienced an unusually large melt extent on the Greenland Ice Sheet (Mote, 2007; Tedesco, 2007; Mernild et al., 2009).

Background

Increased melt has been measured on the Greenland Ice Sheet using both microwave data (Mote and Anderson, 1995; Abdalati and Steffen, 2001; Steffen et al., 2004) and infrared (IR) data (Wang and Key, 2003 and 2005; Comiso, 2006; Hall et al., 2008a). These studies have largely been accomplished using individual sensors such as the passive-microwave instrument on the Scanning Multichannel Microwave Imager (SSM/I), surface-temperature data from the Advanced Very High Resolution Radiometer (AVHRR), MODIS and scatterometer data from QS. Mass loss of the ice sheet has also been reported using aircraft and ICESat laser altimetry (Krabill et al., 2004; Zwally et al., 2005), and Gravity Recovery and Climate Experiment (GRACE) data (Luthcke et al., 2006). Krabill et al. (2004) found thinning along the ice sheet margins and some thickening at the higher elevations which has since been confirmed by independent studies using different instruments (see, for example, Luthcke et al., 2006).

93 There has also been a great deal of work using satellite remote sensing to measure melt
94 extent (for example, Wismann, 2000; Abdalati and Steffen, 2001; Nghiem et al., 2001;
95 Steffen et al., 2004; Fettweis et al., 2007; Mote, 2007; Tedesco, 2007; Wang et al., 2007;
96 Hall et al., 2008a; Tedesco et al., 2008; Sharp and Wang, 2009), clear-sky surface
97 temperature (Stroeve and Steffen, 1998; Comiso et al., 2003 and 2006; Hall et al., 2008a
98 & b) and albedo (Nolin and Stroeve, 1997; Stroeve et al., 1996, 1997, 2005 & 2006;
99 Nolin and Payne, 2007), and changes in melt-related surface characteristics of the
100 Greenland Ice Sheet. Specifically regarding the 2007 melt season, Mote (2007) showed
101 that there were large areas of anomalously-high melt frequency in the summer of 2007,
102 south of 70°N, and Hall et al. (2008a) showed that some drainage basins are experiencing
103 earlier melt initiation in southern Greenland. Some details of the algorithms and products
104 used in this work follow.
105
106
107 **Theoretical Considerations**
108
109 *Emissivity and Land-Surface Temperature (LST).* Emissivity is an intrinsic property of
110 the surface and is independent of the temperature. (See Hook et al. (2007) for further
111 discussion.) The surface emissivity is defined as the ratio of the actual radiance emitted
112 by a given surface to that emitted by a perfect radiator at the same kinetic temperature.
113 Salisbury et al. (1994) show that snow emissivity departs significantly from perfect
114 radiator behavior in the 8 – 14 μm part of the spectrum. Emissivity of snow varies with
115 liquid water content and snow grain size especially at larger grain sizes (Salisbury et al.,

116 1994; Wald, 1994; Hori et al., 2006). To obtain snow or ice LST with an accuracy of
117 0.1°C, the emissivity must be known to within 0.1% (Stroeve et al., 1996).
118
119 *Albedo.* Snow has a very high reflectance in the visible (VIS) wavelengths (0.4 – 0.7
120 μm), up to nearly 100% at the shortest visible wavelengths, but a much lower reflectance
121 in the near-IR (NIR) (0.7 – 2.5 μm) and short-wave IR (SWIR) wavelengths, even near
122 zero around 1.6 μm. In the NIR, snow is very sensitive to grain size changes, thus albedo
123 decreases when grain size increases (Choudhury and Chang, 1979), and melting enhances
124 grain growth (Dozier et al., 1981). In fact, broadband snow albedo can decrease by
125 >25% within a few days after grain growth begins (Nolin and Liang, 2000).
126
127 *Scatterometry.* A scatterometer is a stable and accurate radar. It transmits
128 electromagnetic waves toward a target and measures backscatter, characterizing the
129 scattering of the waves by the target back to the radar. The snow scattering physics have
130 been modeled by a number of researchers (e.g., Tsang et al., 1985; Ulaby et al., 1981;
131 Nghiem et al., 1995). With a wavelength of 2.24 cm in free space (corresponding to a Ku-
132 band frequency of 13.4 GHz), QS backscatter is highly sensitive to snow wetness,
133 allowing Ku-band backscatter to be used for snowmelt detection (Nghiem and Tsai,
134 2001; Nghiem et al., 2001).
135
136 This is because, in wet snow, liquid water (no salinity) has an imaginary part of about 38 ε_0,
137 approximately 19,000 times larger than that of non-melting ice (Klein and Swift, 1977,
138 Tiuri et al., 1984). Furthermore, the large difference in the imaginary part of the

permittivity of dry and wet snow signifies that Ku-band waves can effectively penetrate the surface layer of refrozen snow to detect subsurface wet snow due to an internal snow temperature profile that has not yet reached the freezing point.

Data Products from MODIS and QuikSCAT

Instruments. MODIS is a 36-channel, polar-orbiting, across-track scanning spectroradiometer that images all areas on Earth every 1 – 2 days (Barnes et al., 1998). The first MODIS was launched on the Terra satellite in December 1999 and the second MODIS was launched on the Aqua satellite in May 2002. The MODIS instruments have seven spectral bands in the 0.4 – 2.5 μm range that are relevant for calculation of spectral albedo at either 250- or 500-m spatial resolution. IR channels 31 and 32 (Table 1), are used to calculate daily LST at 1-km spatial resolution.

Table 1. MODIS bands used in this work*.

MODIS band	Bandwidth (μm)	Product
1	620 – 670	MOD10A1 & MCD43 (albedo)
2	841 – 876	MOD10A1 & MCD43 (albedo)
3	459 – 479	MOD10A1 & MCD43 (albedo)
4	545 – 565	MOD10A1 & MCD43 (albedo)

5	1230 – 1250	MOD10A1 & MCD43 (albedo)
6	1628 – 1652	MOD10A1 & MCD43 (albedo)
7	2105 – 2155	MOD10A1 & MCD43 (albedo)
31	10.78 – 11.28	MOD11 (LST)
32	11.770 – 12.270	MOD11 (LST)

*Additional bands (not shown) are used in the input products for the products listed; an example is the MODIS cloud mask (MOD35) which is input to MOD10A1, MCD43 and MOD11.

The SeaWinds scatterometer aboard the QS satellite was launched in June 1999 and has been collecting backscatter data over a swath of 1400 km for the horizontal polarization (H) and 1800 km for the vertical polarization (V). QS acquires backscatter data over the entire island of Greenland two times per day. There are two backscatter products in the QS science dataset with different spatial resolutions (Jet Propulsion Laboratory, 2006). The "egg" data backscatter product has a resolution of 25 km, and the "slice" data have a sub-footprint resolution of about 12 km (Jet Propulsion Laboratory, 2006). The egg data have a higher accuracy and are used in this work for detection and mapping of melt on the ice sheet.

Daily MODIS land-surface temperature (LST) product (MOD11A1). We use the 1-km pixel resolution MODIS LST standard daily product (MOD11A1) of Wan et al. (2002) from Collection-5 reprocessing (Wan, 2008), which provides surface temperatures over

175 the Earth's land areas under clear-sky conditions. The LSTs over snow and ice are
176 accurate to within ±1°C (Wan et al., 2002; Hall et al., 2008b). Relative to other satellite
177 LST results from the Advanced Spaceborne Thermal Emission and Reflection
178 Radiometer (ASTER) and Landsat Enhanced Thematic Mapper Plus (ETM+)
179 instruments, Hall et al. (2008b) show relative agreement of ±0.5°C. We do not know if
180 the accuracy of the MOD11A1-derived LSTs varies with temperature. For example, is
181 the accuracy higher, lower or equal at 0° and -20°C over ice and snow? This is an
182 interesting research question that should be pursued. Nevertheless, the ±1°C accuracy
183 reported by Wan et al. (2002) seems reasonable at a variety of ice-surface LSTs, and may
184 be a conservative accuracy estimate at ice-surface LSTs of –15 to 0°C based on work by
185 Hall et al. (2008b).
186
187 To determine the LST from an instrument that has two IR channels, one must correct for
188 absorption and reemission of radiation by atmospheric gases, predominately water vapor.
189 The "split-window" method is widely used to achieve some correction for atmospheric
190 effects because the measured temperature difference between the two IR channels is
191 proportional to the amount of water vapor in the atmosphere (Key and Haefliger, 1992).
192 To compute the LST to develop the MOD11_L2 product, the emissivity must be
193 prescribed. (MOD11_L2 is a Level 2 swath product.) For bands 31 and 32, the
194 emissivities used in the algorithm to compute LST over the Greenland Ice Sheet are
195 0.993 (for band 31) and 0.990 (for band 32), and do not vary seasonally nor with viewing
196 angle.
197

198 Wan et al. (2002) calculated coefficients in the generalized split-window LST algorithm
199 by interpolation on a set of multidimensional look-up tables obtained by linear regression
200 of MODIS simulation data from radiative-transfer calculations over a wide range of
201 surface and atmospheric conditions. The following MODIS products are input to the
202 MOD11_L2 LST algorithm: sensor radiance (MOD021km), geolocation (MOD03), cloud
203 mask (MOD35_L2), atmospheric temperature and water vapor (MOD07_L2), land-cover
204 (MOD12Q1) and snow cover (MOD10_L2). For this work, a pixel is considered "melt"
205 when the LST $\geq$ -1°C and this simple binary algorithm constitutes the LST melt
206 "product."
207
208 **Albedo products.**
209 *Daily MODIS snow albedo standard product (MOD10A1).* The daily MODIS snow
210 albedo product is a data layer in the snow-cover product, MOD10A1 (Riggs et al., 2006;
211 Hall and Riggs, 2007). The daily snow albedo product was developed by Klein and
212 Stroeve (2002), with heritage from the work of Nolin and Stroeve (1997), Stroeve et al.
213 (1997) and Liang (2000). The product was designed to provide global daily broadband
214 albedo measurements for areas mapped as snow by the MODIS snow algorithm to
215 augment the MODIS 16-day albedo product (MCD43) that currently provides 8-day
216 maps of albedo globally at 500-m resolution (Schaaf et al., 2002) using both Terra and
217 Aqua MODIS data (see section below). MOD10A1 provides more frequent, though less
218 robust, albedo maps than does the MCD43 product. We use MOD10A1 for this work
219 instead of MCD43, because MOD10A1 has a higher temporal resolution, and because
220 absolute albedo values are not required.

To develop the MOD10A1 product, snow albedo is only calculated under clear-sky conditions as determined using the MODIS cloud mask, MOD35 (Ackerman et al., 1998; Platnick et al., 2003). A narrowband or spectral reflectance is calculated for each of the seven MODIS "land" bands (Table 1), then combined into a spectrally-integrated broadband albedo. Snow is treated as an anisotropic surface (Klein and Stroeve, 2002). Albedo is calculated using various inputs such as the MODIS surface reflectance product (MOD09), land cover product (MOD12Q1), and a Digital Elevation Model (DEM) (Klein and Stroeve, 2002). Models of the Bidirectional Reflectance Distribution Function (BRDF) of snow are created using the discrete-ordinate radiative transfer (DISORT) model of Stamnes et al. (1988) to correct for anisotropic scattering effects over non-forested surfaces.

Several validation efforts have shown that the MODIS daily snow albedo products are useful over large, flat areas. Stroeve et al. (2006) assessed the accuracy of the MOD10A1 (Terra) and MYD10A1 (Aqua) daily snow albedo products over the Greenland Ice Sheet. They compared the products with surface albedo measurements on the ice sheet from five AWS during the summer of 2004, and found general agreement of the MODIS measurements with the station data. RMSE for the MOD10A1 was 0.067, and 0.075 for MYD10A1. Tekeli et al. (2006) studied the MOD10A1 product in the mountains of the Karasu Basin in the headwaters of the Euphrates River in eastern Turkey, and found that the MOD10A1 product overestimated albedo by ~10% compared to in-situ measurements. Additional work by Sörman et al. (2006) showed the

MOD10A1 product to be good under conditions of low relief and deep snow cover but results were found to be unreasonable in areas with rugged relief, shallow snow cover and over anisotropic surfaces such as forests that were assumed (in the MODIS daily snow albedo algorithm) to be Lambertian.

16-day MODIS standard BRDF/Albedo product (MCD43C3). The focus of this paper is on the relative change in albedo in relation to melt characteristics rather than on the absolute value of albedo per se. Thus, the absolute calibration of the different albedo products is beyond the scope of this paper but we compare the state-of-the-art albedo product from MODIS (MCD43) with MOD10A1, to address the suitability of MOD10A1 for monitoring daily albedo of the ice sheet (also see Methodology section).

The MODIS BRDF/Albedo product uses all cloud-free, directional surface reflectances (MOD09) available over a 16-day period to retrieve an appropriate form of the RossThickLiSparseReciprocal BRDF model every 8 days at a 500-m resolution (Lucht et al., 2000; Schaaf et al., 2002 & 2008). A high-quality retrieval is only possible when sufficient cloud-free observations that adequately sample the viewing hemisphere are available. If only a very limited number of observations can be used, then the algorithm relies on a backup method where static field-based BRDFs are used as a priori information and coupled with the few observations to estimate the albedo. For the present work, we used the black-sky albedo (BSA) product, MCD43C3, which is provided at 0.5°-resolution on a latitude/longitude grid. (MCD refers to the MODIS combined Terra and Aqua product.) BSA is directional hemispherical reflectance. Also

267 see http://www-modis.bu.edu/brdf/ for further information on the MODIS BRDF/Albedo
268 products.
269
270 The accuracy of the 16-day albedo products over snow and ice surfaces has been studied.
271 Stroeve et al. (2005) found that the MOD43 albedo product retrieves snow albedo with an
272 average RMSE of 0.07 as compared to the station measurements, which have an RMSE
273 uncertainty of 0.035. Greuell et al. (2007) validated the 1-km resolution black-sky
274 MODIS Terra 16-day albedo product, MOD43B3, over a glacier in Svalbard using in-situ
275 data. They found that the highest-quality albedo data in MOD43B3 provided an RMSE
276 of 0.04.
277
278 In addition to the validation studies discussed earlier, we compared the MOD10A1
279 products with a daily version of the MODIS BRDF/Albedo standard product
280 (MCD43C3) using the "backup" algorithm approach developed by Strugnell and Lucht
281 (2001). This was done to further assess the accuracy of MOD10A1 for the present study.
282 In general, MOD10A1 gives somewhat higher albedo values than does MCD43B3,
283 especially in northern Greenland, and along the western margin of the ice sheet. The
284 greatest differences in albedo are found in northern Greenland, and range generally from
285 >0.1 to ~0.2 meaning that MOD10A1 provides higher values in those areas (Hall et al.,
286 2009). Parts of the ice sheet in southern Greenland show slightly higher albedo values in
287 the MCD43B3 product compared to MOD10A1. Though the absolute accuracy of the
288 albedo in MOD10A1 has not been assessed fully with respect to in-situ data (Stroeve et
289 al., 2006; Greuell et al., 2007) and MCD43C3 (Hall et al., 2009), the relative accuracy of

290 the MOD10A1 product is excellent over the ice sheet, and the relative accuracy is what is
291 most relevant to this work.
292
293 *Daily QuikSCAT melt special product*. The diurnal difference method was developed by
294 Nghiem et al. (2001) to monitor the snowmelt process. The algorithm is based on diurnal
295 backscatter difference, a relative quantity between morning and afternoon measurements
296 in half a day to identify current melt, reduced melt, or refreezing conditions (Steffen et al,
297 2004; Nghiem et al., 2005). The QS diurnal algorithm does not require the snow to be
298 completely refrozen (zero liquid water) in the early morning. QS can detect melt as long
299 as there is a differece in the amount of meltwater in snow between morning and evening,
300 causing a difference in the diurnal backscatter. For the case of light melt when there may
301 be some daytime meltwater that fully refreezes during the night (no meltwater in snow),
302 QS sensitivity for melt detection is maintained due to the large difference, by more than
303 three orders of magnitude, in the imaginary part of solid ice and that of liquid water.
304
305 The diurnal method is based on the relative backscatter difference and not on absolute
306 backscatter. With this relative difference approach, the advantages include independence
307 from: absolute backscatter for different snow classes and snow conditions; scatterometer
308 long-term gain drift; orbital changes of the satellite; and cross-calibration between QS
309 and future satellite scatterometers. It also allows the detection of both snowmelt and
310 refreezing. These advantages are not possible with a melt detection method based on a
311 threshold of absolute backscatter, which is dependent on snow grain size, density,
312 accumulation, and ice layer formation created in previous melt seasons (Nghiem et al.,

313 2005). Therefore, the use of the absolute backscatter is inherently complicated and may
314 lead to biases and inconsistencies both in space and time.
315
316 Regarding data resolution, the QS egg data at 25-km resolution have the highest
317 accuracy (0.2 dB for 3σ) for melt detection, which is better than the slice data at 12-km
318 resolution with a lower accuracy resulting in more melt misclassification. A higher
319 resolution of QS data can also be derived with the deconvolution method, however, it
320 requires that the backscatter remains unchanged in each high-resolution pixel during the
321 period of data acquisition (period of a day to a week depending on the scale of the
322 enhanced resolution) used in the resolution enhancement process as stated by Early and
323 Long (2001). This requirement invalidates the use of QS data at a high resolution
324 obtained by the deconvolution method for snowmelt detection because backscatter can
325 change significantly (by as much as an order of magnitude or more) within a few hours or
326 between ascending and descending passes in half a day when snowmelt occurs (Nghiem
327 et al., 2001 and 2005; Steffen et al., 2004). Furthermore, the deconvolution method also
328 needs the merging of data from both ascending and descending passes to have a sufficient
329 number of data samples to significantly enhance the resolution. In that case, one is
330 forced to use the method based on backscatter threshold, leading to inherent
331 inconsistencies and biases.
332
333 We implement here a simple additional step to require that melt occurs at a given pixel in
334 two consecutive days for the pixel to be identified as a melt pixel using QS egg data.
335 This product is called the "QS consistent melt" product (QCM) to distinguish it from the

336 "QS transient melt" product (QTM) when a pixel is classified as melt as long as a
337 transient melt is detected in a single day. Compared to QTM, QCM reduces the inclusion
338 of isolated melt events due to transient weather conditions such as warm air advection
339 associated with storms from the south or warm fronts from the ocean. With the exclusion
340 of transient isolated melt cases, the QCM melt extent is smaller than the corresponding
341 QTM extent. QTM was used to study transient melt events in the dry snow facies of the
342 Greenland Ice Sheet in the anomalous melt season of 2002, and the results indicate that
343 such isolated melt events are short lived and infrequent (~1 day) (Steffen et al., 2004;
344 Nghiem et al., 2005). When the difference between QTM and QCM (QTM-QCM) is
345 used, the variability of isolated or transient melt events can be quantified. This can be
346 related to sensible heat advection and synoptic atmospheric dynamics, which is planned
347 for future study. However, for this work, the use of the QCM product is necessary to
348 allow a consistent comparison with the MODIS melt detection algorithm.
349
350 **Methodology**
351
352 All MODIS and QS data were registered to an Albers conical equal-area projection.
353 Daily (MOD10A1) albedo maps were produced, and the MODIS LST and QS melt
354 product results were blended into a single grid. Using the QS melt product along with the
355 MODIS LST melt product, various categories of melt are provided in the blended maps:
356 1) no melt, or "snow," either MODIS LST or QS maps (shown as "grey" on the blended
357 maps and called "Both Snow"); 2) melt on both MODIS LST maps and QS (shown as
358 "red" and called "Both Melt"); 3) melt on the MODIS LST map and "Reduced Melt" on

359 the QS map (shown as "orange" and called "MODIS Melt/QS Reduced Melt"); 4) QS-
360 derived refrozen snow (shown as "purple hatched" and called "QS Refrozen Snow"); and
361 5) snow on MODIS and melt on QS (shown as "blue" and called "MODIS Snow and QS
362 Melt").
363
364 "Reduced melt" means that QS algorithm detects melt, but the rate or intensity of melt is
365 lower compared to the previous day's melt conditions. Since the QS algorithm detects
366 melt based on differing amounts of liquid water in snow (i.e. snow wetness) between
367 morning and afternoon, if there is a smaller diurnal change in backscatter (i.e., less
368 difference in liquid water content) relative to a larger backscatter change (> 1dB) in
369 previous days, it means that there is less daytime heating and thus less melting, and
370 consequently a slower melt rate (which is thus called "Reduced Melt" on the QS melt
371 product).
372
373 A series of transects from west to east was developed to illustrate the location of changes
374 in albedo (from MOD10A1) with respect to the melt categories on the blended maps.
375 Elevation is derived from the DEM of Bamber et al. (2001). The location (in km) on the
376 x-axis in each transect figure represents number of kilometers from the beginning of the
377 transect, from west to east.
378
379 To identify the geophysical meaning of the melt determined by the MODIS-QS
380 composite map, we investigate seasonal melt evolution over various melt regions of the
381 Greenland Ice Sheet, from incipient through active melt, to freeze-up. This approach

382 allows us to tie the MODIS-QS blended melt classes to physical parameters such as
383 elevation, temperature and albedo.
384
385 We also analyze maximum melt for the 2007 melt season from MODIS LST and QS, and
386 compare the melt-season results from both products on a single map. And we produced a
387 map of minimum albedo for the 2007 melt season to compare with the combined LST-QS
388 seasonal melt map.
389
390 The map of minimum albedo was developed in the following way. First, sharp dips in
391 the albedo were minimized. The sharp albedo dips are generally caused by unmasked
392 clouds, but may also be related to the presence of melt ponds (see Box and Ski, 2007;
393 Sneed and Hamilton, 2007). Sneed and Hamilton (2007) discuss melt ponds and
394 extensive areas of non-ponded surface water. These areas could influence the albedo
395 within the MODIS pixel. To eliminate or minimize inclusion of albedo dips, each pixel
396 value of albedo was compared to pixels from the two previous days of conservatively
397 non-cloudy data. If the current day albedo was a new minimum and had a lower value
398 than that of the two previous days by 10 percentage points or more, then it was
399 considered a "dip" and eliminated. If the albedo were lower by less than 10 percentage
400 points for both of the previous two good days, then it was considered an acceptable value,
401 and the current day's albedo was recorded as the lowest albedo value for that pixel.
402
403

404 **Results**

405

406 The MODIS daily snow albedo product is the most sensitive of the three products to
407 surface changes. The QS melt product is the most sensitive to surface *and* near-surface
408 (centimeters to decimeters) melt intensity, and though the MODIS LST product is not
409 sensitive to melt intensity because of the binary nature of the algorithm used for this
410 work, it is still highly effective in detecting active surface melting, and can be used alone,
411 or in conjunction with other data to detect surface melt/freeze boundaries.

412

413 *Incipient melt phase.* Lowering of the albedo on the ice sheet was first seen around 22
414 March (where the albedo decreased from ~95% to as low as ~80% in the southern part of
415 the ice sheet). The LST-QS blended maps do not show sustained melt until late May /
416 early June 2007 (on the periphery of the ice sheet), so it is highly unlikely that the
417 MODIS daily snow albedo algorithm, MOD10A1, was detecting surface melt in March
418 and April in the higher-elevation parts of the ice sheet. A likely explanation for the
419 albedo decrease beginning in mid-March is that shadows from sastrugi and other wind-
420 sculpted snow features began to change, causing a reduction in the albedo; this is
421 particularly likely at high solar-zenith angles. According to Stroeve et al. (2005),
422 undulations and wind-sculpted features such as sastrugi, represent altered snow grain
423 sizes and introduce shadowing effects to the snow surface that can lower the albedo.

424

425 *Active melt phase.* Melt is often detected first with the QS product and soon after with
426 the MODIS LST. On 1 June 2007, in the southwestern margin of the ice sheet, QS shows

427 extensive melt on the ice sheet margin (red, oragnge and blue areas on blended map in
428 Figure 1a), with less melt observed by the MODIS LST product. On the next day, 2
429 June, the extent of melt, as observed by the MODIS LST product, increased (red and
430 orange areas in Figure 1b). By 3 June, both the LST and QS products show extensive
431 melt in the southwestern margin of the ice sheet (Figure 2b). The albedo map (Figure 2a)
432 also indicates melting as evidenced by the significantly reduced albedos (<75%) along
433 the southwestern margin of the ice sheet as compared to inland values. Though not
434 shown, a similar pattern is evident for 26 - 27 June, 1 - 2 July and 11 - 12 August, as well
435 as on other dates, where QS detects melt first, and then the MODIS LST product detects
436 melt after a 1- to 2-day delay. This delay may be caused by one or a combination of three
437 physical reasons: (1) meltwater may be present below a frozen surface; this can be
438 detected only by QS; or (2) QS is more sensitive to melt detection than is the MODIS
439 LST; or (3) MODIS may be missing surface melt if it is not mapping the area at the
440 warmest time of the day, while the QS algorithm detects any melt between 06:00 and
441 18:00 local time (data at the outer sides of each swath can be earlier or later than the local
442 time of the data acquired at the swath center due to the large swath width).
443
444 On 3 June on the eastern part of the ice sheet, the east transect plot (Figure 2c) illustrates
445 a dramatic drop in albedo (from ~83 to ~25%) at the snowline from the frozen to the
446 melted parts of the ice sheet surface between ~42 and 52 km from the beginning of the
447 transect (see change from grey to orange area). The solid black line represents albedo.
448 All of the products respond to a sudden change from a frozen surface to a melted surface
449 from west to east. Note the sharp drop in elevation coincident at this location as well,

450 which is most probably the controlling mechanism for the change in surface state. The
451 dashed black line represents elevation.
452
453 Turning to the southwest transect, also on 3 June, we see albedo variability that is likely
454 caused by inhomogeneity in surface melt within the area of melt on the blended map
455 (orange and red areas in transect in Figure 2d). Surface melt features such as melt ponds
456 cause changes in albedo between ~10 to 91 km from the beginning of the transect. Snow
457 albedo increases from a location on the transect, from ~24 to 137 km, to a maximum of
458 ~80%, in response to smaller grain sizes at the higher elevations. Note the somewhat
459 abrupt increase in albedo before 114 km when melted snow as detected by QS (blue)
460 becomes frozen (grey), a likely result of decreased surface snow grain size.
461
462 MOD10A1 is sensitive enough to grain size changes so that it can detect conditions
463 associated with different melt intensities. The lowest albedos (<25%) observed in 2007
464 correspond to bare glacier ice. The QS and MODIS LST melt products do not distinguish
465 bare ice and/or impurity-rich ice from snow-covered ice when the surface is dominated
466 by a wet layer. The distinct albedo zones in southwestern Greenland seen in Figure 2a,
467 and in Figure 3a on 5 July indicate sustained melt features and they correspond with the
468 MODIS LST and QS melt when both show active melting (red on the blended maps in
469 Figure 3b). This is probably an area containing bare ice on 5 July.
470
471 On 5 July 2007, a gradual lowering of the albedo is seen in the east transect (Figure 3c)
472 from the zone of snow (grey) where the albedo is ~85%, to the zone of refrozen snow

473 (purple hatched area over grey) accompanying a grain-size increase from frozen snow to
474 refrozen snow. Albedo continues to decrease in the zone of refrozen snow. Then there is
475 a sharp drop in albedo (from ~75 to 65%) from the zone of refrozen snow to the zone of
476 wet snow / reduced melt (orange) (Figure 3c) at a location of ~ 304 km.
477
478 Also on 5 July, Figure 3d, a transect in southwestern Greenland, indicates a range of
479 albedos (from ~<35 to 70%) within the QS-MODIS zone of active melting (red) implying
480 albedo sensitivity to melt intensity (or possibly to impurity-rich ice) whereas the QS and
481 LST melt algorithms simply identify this area as melt. Also in the southwest transect
482 (Figure 3d), albedo rises sharply from an area of melt which is detected by both MODIS
483 and QS (red), to melt detected by QS only (blue) at 84 km where the surface is frozen
484 according to the LST product. The albedo continues to increase, but gradually from
485 melted (blue) to refrozen snow (purple hatched over grey) and then to the region of dry
486 snow (grey), again probably in response to smaller grain sizes from melted and refrozen
487 to dry snow where no melt was detected by LST and QS.
488
489 By 4 August 2007 (Figure 4a, b & c), most of the inland parts of southern Greenland are
490 refrozen (see purple hatched over grey area on Figures 4b and c), with neither MODIS
491 LST nor QS indicating active melt except near the ice sheet margins. The transect
492 (Figure 4c) across southern Greenland shows that the albedo is abruptly higher at a
493 location of ~35 km, moving eastward from melt detected by both MODIS LST and QS
494 (red) where the albedo is as low as ~30%, to melt detected by QS only (blue) where the
495 albedo rapidly increases to nearly 80%. The MODIS LST and albedo products are

496 consistent here: the large increase in albedo is coincident with the LST product changing
497 from detecting a melted to a frozen surface at ~35 km. In the region of melt observed by
498 QS only (blue) after 35 km, the albedo changed from a low of ~30% to a high of ~78%.
499 The existence of QS subsurface melt is physically consistent with this observation since a
500 refrozen surface can maintain the freezing condition for new snow from either snow drift
501 or snowfall with a higher albedo. The steep elevation increase in this area is likely
502 responsible for changes in surface temperatures and in melt states with different
503 wetnesses corresponding to the relative changes in albedo. Or, the albedo dip at ~35 km
504 may signify the presence of impurity-rich ice (J. Box written communication).
505
506 *Extreme melt episode.* On 13 August 2007 (Figure 5a, b & c) there was a melt event in
507 which active melting is evident on both the LST and QS products (red, orange and blue in
508 southern Greenland in Figure 5b). The MODIS daily snow albedo map, Figure 5a,
509 illustrates lowered albedo in southern Greenland as compared to the previous day,
510 probably due to larger grain sizes resulting from surface melt on 13 August (Figure 6).
511 Albedo along the westernmost part of the transect is shown in Figure 6 for 12 and 13
512 August, with a lowering of the albedo during the melt event on 13 August. Also on 13
513 August, extensive melt is observed at the eastern ice sheet margin (red and orange) in
514 Figures 5b and c.
515
516 A transect extending from west to east across the southern part of the ice sheet is shown
517 in Figure 5c. Steep increases in albedo occur within the melted (red and orange) areas to
518 a maximum of ~75%, resulting from lowered surface temperatures (a transition from a

519 melted to a frozen surface) coincident with steeply increasing elevation (see dashed line).
520 Note the abrupt albedo increase when the MODIS LST product indicates a change from a
521 melted to a frozen surface (from the red to blue areas at the location of just before 231 km
522 in Figure 5c). (This was also noted on Figure 3d.) Again, the consistency of the melt
523 states identified by the LST and QS products [from melt (red), to a frozen surface with
524 subsurface melt (blue), to dry snow (grey)], with the albedo product confirms that a
525 geophysical boundary is identified. Both MODIS products are responding to the abrupt
526 change from a wet to a frozen surface while QS continues to detect melt below the
527 surface (blue) or is responding to melt that occurred sometime during that day
528 approximately between 06:00 and 18:00 local time that was missed by the MODIS
529 products that are based on instantaneous "snapshots" in time, of the surface.
530
531 Hanna et al. (2008) show that the summer of 2007 was the second warmest since 1961,
532 and Mernild et al. (2009) show record melt extent and runoff from the ice sheet in 2007.
533 During the summer of 2007, some locations on the ice sheet experienced as many as 50
534 more days of melt than the 1973 – 2007 average (Mote, 2007). T. Mote (written
535 communication) identified an extensive area of melt on 13 August 2007 in southern
536 Greenland using passive-microwave data that is roughly comparable in size, though
537 larger, than the melt region identified using the MODIS LST map on that same day.
538 Tedesco (2007) also noted an increase in frequency of melt in regions above 2000 m.
539
540 *Maximum melt extent in 2007 melt season.* The maximum extent of melt detected by the
541 MODIS LST (766,184 km^2) and QS (862,769 km^2) melt products is shown in Figure 7.

542 MODIS and QS generally agree (89%) in the detection of seasonal melt extent with about
543 11% larger extent detected by QS. Differences occur at higher elevations farther inland
544 near the boundary of the maximum melt extent. Melt extent reached higher elevations as
545 measured by QS probably because of the capability of the QS to detect sub-surface as
546 well as surface melt. In addition, the peak temperature and melt of the ice sheet probably
547 occurs at about 13:00 – 14:00 local time on most days. The QS diurnal algorithm is
548 based on the presence of melt between 06:00 and 18:00 local time, which includes the
549 hours of peak melting and MODIS swaths from those hours may not always be selected
550 by the MODIS LST algorithm, or the swath observations (which are instantaneous), at
551 those hours might have been cloud obscured. Thus less melt is likely to be detected by
552 the MODIS LST product when those circumstances prevail.
553
554 *Freeze-up phase.* By 27 August 2007 (images not shown), the albedo remained low at
555 the ice margin in both eastern and western Greenland (but it is more pronounced in
556 western Greenland because the ablation zone is wider there); in addition, the MODIS
557 LST map indicates that melt was occurring in those locations, while the QS map indicates
558 reduced melt. As snow continued to fall and as temperatures decreased, the albedo
559 increased and the blended map shows increasingly less melt along the ice margins as the
560 freeze-up period progressed.
561
562
563 **Discussion of uncertainties**
564

565 *Detection of subsurface melt by QuikSCAT.* QS indicates significantly more melting in
566 southern Greenland on 5 July 2007 than does MODIS LST as evidenced by the extensive
567 "blue" area in southern Greenland seen on Figure 3b. Analysis of the LSTs in the blue
568 area indicates that there are large areas where the LSTs are -3° and -2°C which is close to
569 the LST threshold for melt used in this work (≥-1°C). First, QS has a greater sensitivity
570 for detecting melt as discussed previously. In addition, the skin depth for the LST
571 product is only a few mm while the QS can penetrate through the refrozen snow of the
572 surface layer. Therefore it is likely that the surface was frozen over much of the area and
573 that there was internal liquid water content below the surface layer. Further evidence of
574 this can be drawn from the cases where both MODIS products detected a frozen surface
575 while the QS product detected melt (see, for example, the "blue" area in Figure 4c as
576 discussed previously).
577
578 Hoffman et al. (2008) indicate that subsurface melt is often present in a glacial
579 environment. Moreover, van den Broeke et al. (2008) show that radiation penetration can
580 cause the ice to melt below the surface while summer melting can be intermittent due to
581 nighttime surface freezing at higher altitudes (and thus farther inland) of the ice sheet. In
582 Figures 2 to 5, the blue areas (QS melt and MODIS dry snow) are consistently located
583 farther inland at higher latitudes compared to the corresponding red areas (both QS and
584 MODIS melt). This may further explain why melt is detected by QS and not by the
585 MODIS LST.
586

587 *Temporal considerations.* Another uncertainty factor is that the LST product may not be
588 acquired at a time of the day when peak melting occurs, while QS senses the meltwater
589 accumulated during the melt process throughout the day between ~06:00 and 18:00 local
590 time. In the days after 5 July 2007, much of the blue area in Figure 3b becomes mostly
591 red, indicating the agreement of both MODIS and QS in the identification of melt extent
592 as melt progresses. But if melt does not progress, the two products will not necessarily
593 agree, that is, if the surface does not melt.
594
595 *Limitations of the daily snow albedo product.* Comparisons of the MODIS daily snow
596 albedo product, MOD10A1, with the higher-quality MODIS 16-day albedo product,
597 MCD43C3, are somewhat ambiguous as discussed in Hall et al. (2009), and will require
598 much further work to understand. We found generally good correspondence at the lower
599 elevations of the ice sheet and poorer correspondence at the higher elevations between
600 the MOD10A1 and a daily version of MCD43 (the 16-day MODIS albedo product). The
601 relative MOD10A1 albedo values presented in this paper are reasonable and consistent,
602 though the absolute albedo values may not be accurate as compared to the superior
603 MCD43C3 product which is based on more views of the surface (Schaaf et al., 2002).
604 Absolute values are not required to draw the conclusions reported herein.
605
606
607 **Discussion and Conclusions**
608 Researchers use various remote sensing methods to measure melt on the Greenland Ice
609 Sheet. Each method has advantages and limitations. Algorithms based on active

610 microwave instruments, such as from a scatterometer, are very sensitive to melt and melt
611 extent, and can detect liquid water beneath the ice sheet surface but cannot provide high
612 spatial resolution and thus great detail, especially in transition areas such as at the
613 snowline. VIS, NIR and IR data provide images of melt at relatively high spatial
614 resolutions (up to 250 m on a daily basis), but cannot image through cloud cover and are
615 not as sensitive to melt as are the microwave sensors. However, when results from these
616 various sensors are combined, or "blended," then the attributes of each are accentuated
617 and the limitations are downplayed.
618
619 Consistent results from the various products provide confirmation of different melting
620 states on the Greenland Ice Sheet for the 2007 melt season. Both the MODIS and QS are
621 sensitive to melt onset. The MODIS daily albedo product is the most sensitive of the
622 three products for detecting surface changes, but the QS is the most sensitive for
623 detecting liquid water in the surface and near-surface of the ice sheet. Surface changes,
624 detected by the MODIS daily snow albedo product, are not necessarily melt-related, but
625 may be related to wind effects.
626
627 Relative albedo changes in the MODIS daily snow albedo product show snow and ice
628 surface changes, including surface melt intensity. The MODIS daily snow albedo
629 product responds to grain-size changes between areas with more-intense melting (larger
630 grain sizes) and areas characterized by a frozen surface (smaller grain sizes). Once the
631 grain size has increased due to an earlier melt event, albedo may not regain its highest
632 values after the surface becomes frozen again until new snow is deposited in the region

633 by snow drift or snowfall. This explains much of the albedo variability and spatial
634 patterns in refrozen areas.
635
636 Elevation and orientation (surface slope azimuth) play an important role in the melt states
637 of the ice sheet. We did not address orientation in this paper, but using DEM (Bamber et
638 al., 2001), we show that elevation change can be associated with sudden changes in the
639 state of melting on the ice sheet by causing rapid changes in near-surface air temperature
640 and thus surface temperature. In addition, large or sudden changes in near-surface air
641 temperatures and thus LST can be caused by katabatic winds.
642
643 With this suite of melt products from MODIS and QS, we can measure small changes in
644 the surface- and near-surface melt states of the snow and ice on the Greenland Ice Sheet.
645 The products are consistent in identifying physical properties of the complex snowmelt
646 process. The ice sheet responds very quickly to changes in near-surface temperature
647 through surface melting and re-freezing and even sometimes by maintaining liquid water
648 just beneath the surface (detected by the QS product), yet the amount and depth of liquid
649 water beneath the surface needs to be evaluated further by in-situ observations. Also
650 relevant is a quantitative comparison of the MODIS LST, daily albedo and QS melt maps
651 with melt maps produced using passive-microwave data. This is an important follow-up
652 project for future work, not addressed in the present work.
653
654 The products provide remarkably consistent results showing the locations of, and
655 sometimes rapid changes in, boundaries between melted versus frozen surface conditions.

656 This work has demonstrated that these are physically-meaningful "boundaries" and not
657 artifacts of remote sensing data processing. Using these products, we can improve the
658 precision in mapping surface and near-surface melt on the Greenland Ice Sheet to enable
659 improved quantification of meltwater runoff.
660
661
662 **Acknowledgments**
663
664 The authors thank Dr. George Riggs / SSAI for discussions concerning the MODIS daily
665 snow albedo product and comparisons with the MODIS BRDF/Albedo product. We also
666 thank Dr. Zhengming Wan / University of California at Santa Barbara for many valuable
667 discussions about the MODIS Land Surface Temperature product and its validation. We
668 also thank one anonymous reviewer and Drs. Jason Box / Ohio State University and
669 Thomas Mote / University of Georgia, for their very helpful reviews. The work carried
670 out at Goddard Space Flight Center was supported by NASA's Earth Observing System
671 (EOS) Program and the Cryospheric Sciences Program. The research carried out at the
672 Jet Propulsion Laboratory, California Institute of Technology, was also supported by
673 NASA.

674 **References**

675

676 Abdalati, W. and K. Steffen (2001), Greenland ice sheet melt extent: 1979-1999, *J.*
677 *Geophys. Res., 106(D24),* 33,983-33,989.

678

679 Ackerman, S.A., K.I. Strabala, P.W.P. Menzel, R.A. Frey, C.C. Moeller, L.E. Gumley
680 (1998), Discriminating clear sky from clouds with MODIS, *J. Geophys. Res. 103*(D24),
681 32,141-32,157.

682

683 Bamber, J.L., S. Ekholm and W.B. Krabill (2001), A new, high-resolution digital
684 elevation model of Greenland fully validated with airborne laser altimeter data, *J.*
685 *Geophys. Res., 106*(B4), 6733-6745.

686

687 Barnes, W.L., T.S. Pagano and V.V. Salomonson (1998), Prelaunch characteristics of the
688 Moderate Resolution Imaging Spectroradiometer (MODIS) on EOS-AM1, *IEEE Trans.*
689 *Geosci. and Rem. Sens., 36*(4), 1088-1100.

690

691 Box, J. E. (2002), Survey of Greenland instrumental temperature records: 1873-2001, *Int.*
692 *Jour. Clim., 22*, 1829-1847.

693

694 Box, J.E. and K. Ski (2007), Remote sounding of Greenland supraglacial melt lakes:
695 implications for subglacial hydraulics, *Jour. Glaciol., 53*(181), 257-265.

696

697 Choudhury, B.J. and A.T.C. Chang (1979), Two-stream theory of reflectance of snow,
698 *IEEE Trans. Geosci. Rem. Sens., GE-17*(3), 63-68.
699
700 Comiso, J.C. (2006), Arctic warming signals from satellite observations, *Weather*, *61*(3),
701 70-76.
702
703 Comiso, J., J. Yang, S. Honjo and R.A. Krishfield (2003), Detection of change in the
704 Arctic using satellite and in situ data, *J. Geophys. Res.*, *108*(C12), 3384,
705 doi:10.1029/2002JC001347.
706
707 Dozier, J., S.R. Schneider and D.F. McGinnis, Jr. (1981), Effect of grain size and
708 snowpack water equivalence on visible and near-infrared satellite observations of snow,
709 *Water Resour. Res., 17,* 1213-1221.
710
711 Early, D.S., and Long, D.G. (2001), Image reconstruction and enhanced resolution
712 imaging from irregular samples, *IEEE Trans. Geosci. Rem. Sens.*, *39*(2), 291-302.
713
714 Fettweis, X., J.-P. van Ypersele, H. Gallée, F. Lefebre and W. Lefebre (2007), The 1979
715 – 2005 Greenland ice sheet melt extent from passive microwave data using an improved
716 version of the melt retrieval XPGR algorithm, *Geophys. Res. Lett., 34*,
717 doi:10.1029/2006GL028787, 2007.
718

719 Gregory, J.M., P. Huybrechts and S.C.B. Raper (2004), Threatened loss of the Greenland
720 ice sheet, *Nature*, *428*, 616 (8 April 2004).
721
722 Greuell, W., J. Kohler, F. Obleitner, P. Glowacki, K. Melvold, E. Bernsen and J.
723 Oerlemans (2007), Assessment of interannual variations in the surface mass balance of
724 18 Svalbard glaciers from the Moderate Resolution Imaging Spectroradiometer/Terra
725 albedo product, *J. Geophys. Res.*, *112*, doi:10/1029/2006/JD007245.
726
727 Hall, D.K. and Riggs, G.A. (2007), Accuracy assessment of the MODIS snow-cover
728 products, *Hydrol. Proc., 21,* 1534-1547.
729
730 Hall, D.K., R.S. Williams, Jr., S.B. Luthcke and N.E. DiGirolamo (2008a), Greenland Ice
731 Sheet surface temperature, melt and mass loss: 2000 – 2006, *Jour. Glaciol.*, *54*(184), 81-
732 93.
733
734 Hall, D.K., J.E. Box, K.A. Casey, S.J. Hook, C.A. Shuman and K. Steffen (2008b),
735 Comparison of satellite-derived and in-situ observations of ice and snow surface
736 temperatures over Greenland, *Rem. Sens. Environ.*, *112*(10), 3739-3749,
737 doi:10.1016/j.rse.2008.05.007.
738
739 Hall, D.K., C.B. Schaaf, Z. Wang and G.A. Riggs (2009), Enhancement of the MODIS
740 daily snow albedo product, *Proceedings of the 89th American Meteorological Society*
741 *Annual Meeting,* Phoenix, Ariz., 11-15 January 2009.

742

743 Hanna, E., P. Huybrechts, K. Steffen, J. Cappelen, R. Huff, C. Shuman, T. Irvine-Fynn,
744 S. Wise and M. Griffiths (2008), Increased runoff from melt from the Greenland ice
745 sheet: A response to global warming, *Jour. Clim.*, doi: 10.1175/2007JCLI1964.1.

746

747 Hoffman, M.J., A.G. Fountain, and G.E. Liston (2008), Surface energy balance and melt
748 thresholds over 11 years at Taylor Glacier, Antarctica, *J. Geophys. Res.*, 113, F04014,
749 doi:10.1029/2008JF001029.

750

751 Hook, S.J., R.G. Vaughan, H. Tonooka and S.G. Schladow (2007), Absolute Radiometric
752 In-Flight Validation of Mid Infrared and Thermal Infrared Data from ASTER and
753 MODIS on the Terra Spacecraft Using the Lake Tahoe, CA/NV, USA, Automated
754 Validation Site, *IEEE Trans. Geosci. Rem. Sens.*, *45*, 1798-1807.

755

756 Hori, M., T. Aoki, T. Tanikawa, H. Motoyoshi, A. Hachikubo, K. Sugiura, T.J. Yasunari,
757 H. Eide, R. Storvold, Y. Nakajima and F. Takahashi (2006), In-situ measured spectral
758 directional emissivity of snow and ice in the 8 – 14 μm atmospheric window, *Rem. Sens.*
759 *Environ., 100*, 486-502.

760

761 Jet Propulsion Laboratory (2006), *QuikSCAT Science Data Product User's Manual*, Jet
762 Propulsion Laboratory Document D-18053-RevA, 90 pp. Pasadena, CA. Available at
763 ftp://podaac.jpl.nasa.gov/ocean_wind/quikscat/L2B/doc/QSUG_v3.pdf

764

765 Key, J. and M. Haefliger (1992), Arctic ice surface temperature retrieval from AVHRR
766 thermal channels, *J. Geophys. Res., 97*(D5), 5885-5893.
767
768 Klein, L. A., and C. Swift (1977), An improved model for the dielectric constant of sea
769 water at microwave frequencies, *IEEE Trans. Antennas Propag., AP-25*(1), 104-111.
770
771 Klein, A.G. and J. Stroeve (2002), Development and validation of a snow albedo
772 algorithm for the MODIS instrument, *Ann. Glaciol., 34,* 45-52.
773
774 Krabill, W., E. Hanna, P. Huybrechts, W. Abdalati, J. Cappelen, B. Csatho, E. Frederick,
775 S. Manizade, C. Martin, J. Sonntag, R. Swift, R. Thomas, W. and J. Yungel (2004),
776 Greenland Ice Sheet: Increased coastal thinning, *Geophys. Res. Lett., 31,* L24402,
777 doi:10/1029/2004GL021533.
778
779 Liang S. (2000), Narrow to broadband conversion of land surface albedo I: algorithms,
780 *Rem. Sens. Environ., 76,* 213-238.
781
782 Lucht, W., C.B. Schaaf and A.H. Strahler (2000), Theoretical noise sensitivity of BRDF
783 and albedo retrieval from the EOS-MODIS and MISR sensors with respect to angular
784 sampling, *Int. Jour. Rem. Sens., 21*, 81-98.
785

786 Luthcke, S.B., H.J. Zwally, W. Abdalati, D.D. Rowlands, R.D. Ray, R.S. Nerem, F.G.
787 Lemoine, J.J. McCarthy and D.S. Chinn (2006), Recent Greenland ice mass loss by
788 drainage system from satellite gravity observations, *Science,* 19 October 2006,
789 *314*(5803), 1286-1289.
790
791 Mernild, S.H., G.E. Liston, C.A. Hiemstra and K. Steffen (2009), Record 2007 Greenland
792 Ice Sheet melt extent and runoff, *Eos*, *90*(2), 13-14.
793
794 Mote, T.L. and M.R. Anderson (1995), Variations in snowpack melt on the Greenland ice
795 sheet, based on passive-microwave measurements, *Jour. Glaciol., 41*, 51-60.
796
797 Mote, T. (2007), Greenland surface melt trends 1973 – 2007: evidence of a large increase
798 in 2007, *Geophys. Res. Lett., 34,* L22507, doi:10.1029/2007GL031976.
799
800 Nghiem, S. V., R. Kwok, S. H. Yueh, J. A. Kong, M. A. Tassoudji, C. C. Hsu and R. T.
801 Shin (1995), Polarimetric scattering from layered media with multiple species of
802 scatterers, *Radio Sci.*, 30(4), 835-852.
803
804 Nghiem, S., K. Steffen, R. Kwok and W.-Y. Tsai (2001), Detection of snowmelt regions
805 on the Greenland ice sheet using diurnal backscatter change, *Jour. Glaciol., 47*(159),
806 593-547.

807

808 Nghiem, S.V., and W.Y. Tsai (2001), Global snow cover monitoring with spaceborne
809 Ku-band scatterometer, *IEEE Trans. Geosci. Rem. Sens.*, *39*, 2118-2134.

810

811 Nghiem, S. V., K. Steffen, G. Neumann, and R. Huff (2005), Mapping of ice layer extent
812 and snow accumulation in the percolation zone of the Greenland ice sheet, *J. Geophys.*
813 *Res.*, *110*, F02017, doi:10.1029/2004JF00234.

814

815 Nolin, A.W. and J.C. Stroeve (1997), The changing albedo of the Greenland ice sheet:
816 Implications for climate change, *Ann. Glaciol.,25*, 51-57.

817

818 Nolin, A.W. and S. Liang (2000), Progress in bi-directional reflectance modeling and
819 applications for surface particulate media: snow and soils, *Rem. Sens. Rev., 18,* 307-342.

820

821 Nolin, A.W. and M.C. Payne (2007), Classification of glacier zones in western Greenland
822 using albedo and surface roughness from Multi-angle Imaging SpectroRadiometer
823 (MISR), *Rem. Sens. Environ.,107*, 264-275, doi:10/1016/j.rse.2006.11.004.

824

825 Platnick, S., M.D. King, S.A. Ackerman, W.P. Menzel, B.A. Baum, J.C. Riédi, R.A. Frey
826 (2003), The MODIS cloud products: algorithms and examples from Terra, *IEEE Trans.*
827 *Geosci. Rem. Sens., 41*(2), 459-473.

828

829 Riggs, G.A., D.K. Hall and V.V. Salomonson (2006), *MODIS Snow Products User*
830 *Guide*, http://modis-snow-ice.gsfc.nasa.gov/sugkc2.html .
831
832 Rignot, E., J. E. Box, E. Burgess, and E. Hanna (2008), Mass balance of the Greenland
833 ice sheet from 1958 to 2007, *Geophys. Res. Lett.*, *35*, L20502,
834 doi:10.1029/2008GL035417.
835
836 Salisbury, J.W., D.M. D'Aria and A. Wald (1994), Measurements of thermal infrared
837 spectral reflectance of frost, snow, and ice. *J. Geophys. Res., 99*, 24,235-24,240.
838
839 Schaaf, C.B., F. Gao, A.H. Strahler and 21 others (2002), First operational BRDF, albedo
840 nadir reflectance products from MODIS, *Rem. Sens. Environ.*, *83*(1-2), 135-148.
841
842 Schaaf C., J. Martonchik, B. Pinty, Y. Govaerts, F. Gao, A. Lattanzio, J. Liu, A. Strahler
843 and M. Taberner (2008), Retrieval of Surface Albedo from Satellite Sensors, *in* Advances
844 in Land Remote Sensing: System, Modelling, Inversion and Application, S. Liang (ed.),
845 Springer, ISBN 978-1-4020-6449-4219-243.
846
847 Serreze, M.C., J. E. Walsh, F. S.Chapin III, T. Osterkamp, M. Dyurgerov, V.
848 Romanovsky, W. C. Oechel, J. Morison, T. Zhang and R. G. Barry (2000), Observational
849 evidence of recent change in the northern high-latitude environment, *Climate Change, 46*,
850 159-207.
851

852 Sharp, M. and L. Wang (2009), A Five-Year Record of Summer Melt on Eurasian Arctic
853 Ice Caps, *Jour. Clim., 22*, 133-145, doi: 10.1175/2008JCLI2425.1.
854
855 Sneed, W.A. and G.A. Hamilton (2007), Evolution of melt pond volume on the surface of
856 the Greenland Ice Sheet, *Geophys. Res. Lett., 34*, L03501, doi:10.1029/2006GL028697.
857
858 Sorman, A.U., Z. Akyurek, A. Sensoy, A.A. Sorman and A.E. Tekeli (2006),
859 Commentary on comparison of MODIS snow cover and albedo products with ground
860 observations over the mountainous terrain of Turkey, *Hydrol. Earth Syst. Sci. Discuss., 3,*
861 3655-3673 www.hydrol-earth-syst-sci-discuss.net/3/3655/2006/
862
863 Stamnes, K., S-C Tsay, W. Wiscombe and K. Jayaweera (1988), Numerically stable
864 algorithm for discrete-ordinate-method radiative transfer in multiple scattering and
865 emitting layered media, *Appl. Optics, 27*, 2502-2509.
866
867 Steffen, K. and J. Box (2001), Surface climatology of the Greenland ice sheet: Greenland
868 climate network 1995-1999, *Jour. Geophys. Res., 106*(D24), 33,951-33,964.
869
870 Steffen, K., S.V. Nghiem, R. Huff, and G. Neumann (2004), The melt anomaly of 2002
871 on the Greenland Ice Sheet from active and passive microwave satellite observations,
872 *Geophys. Res. Lett., 31*(20), L2040210.1029/2004GL020444, 2004.
873
874

875 Stroeve, J. and K. Steffen (1998), Variability of AVHRR-derived clear-sky surface
876 temperature over the Greenland ice sheet, *Jour. Appl. Meteorol.*, *37,* 23-31.
877
878 Stroeve, J., M. Haefliger and K. Steffen (1996), Surface temperature from ERS-1 ATSR
879 infrared thermal satellite data in polar regions, *Jour. Appl. Meteorol., 35*(8), 1231-1239.
880
881 Stroeve, J.C., A.W. Nolin and K. Steffen (1997), Comparison of AVHRR-derived and in
882 situ surface albedo over the Greenland ice sheet, *Rem. Sens. Environ., 62*(3), 262-276.
883
884 Stroeve, J.C., J. Box, J. Gao, S. Liang, A. Nolin and C. Schaaf (2005), Accuracy
885 assessment of the MODIS 16-day snow albedo product: comparisons with Greenland in
886 situ measurements, *Rem. Sens. Environ., 94,* 46-60.
887
888 Stroeve, J., J. Box and T. Haran (2006), Evaluation of the MODIS (MOD10A) Daily
889 Snow Albedo Product over the Greenland Ice Sheet, *Rem. Sens. Environ.*, *105,* 155-171,
890 doi:10/1016/j.rse.2006.06.009.
891
892 Strugnell, N.C. and W. Lucht (2001), Continental-scale albedo inferred from ANHRR
893 data, land cover class and field observations of typical BRDFs, *Jour. Clim., 14*, 1360-
894 1376.
895

896 Tedesco, M. (2007), Snowmelt detection over the Greenland ice sheet from SSM/I
897 brightness temperature daily variations, *Geophys. Res. Lett.*, *34*, L02504, doi:
898 10.1029/2006GL028466.
899
900 Tedesco, M., M. Serreze and X. Fettweis (2008), Diagnosing the extreme surface melt
901 event over southwestern Greenland in 2007, *The Cryosphere*, *2*, 159-166.
902
903 Tekeli, A.E., A. Ensoy, A. Sorman, Z. Akyürek, Ü. Sorman (2006), Accuracy assessment
904 of MODIS daily snow albedo retrievals with *in situ* measurements in Karasu basin,
905 Turkey, *Hydrol. Proc., 20*(4), 705-721, doi: 10.1002/hyp.6114.
906
907 Tiuri, M.E., A.H. Sihvola, E.G. Nyfors, and M.T. Hallikainen (1984), The complex
908 dielectric constant of snow at microwave frequencies, *IEEE Jour. Ocean Eng.*, *OE-9*(5),
909 377-382.
910
911 Tsang, L., J.A. Kong, and R.T. Shin (1985), Theory of Microwave Remote Sensing, John
912 Wiley & Sons, New York.
913
914 Ulaby, F. T., R.K. Moore, and A.K. Fung (1981), Microwave Remote Sensing: Active
915 and Passive, Artech House, Massachusetts.
916

van de Wal, R.S.W., W. Greuell, M.R. van den Broeke, C.H. Reijmer and J. Oerlemans (2006), Surface mass balance observations and automatic weather station data along a transect near Kangerlussuaq, West Greenland, *Ann. Glaciol., 42*, 311-316.

van den Broeke, M., P. Smeets, J. Ettema, C. van der Veen, R. van de Wal and J. Oerlemans (2008), Partitioning of energy and meltwater fluxes in the ablation zone of the west Greenland ice sheet, *The Cryosphere, 2,* 179-189.

Wald, A. (1994), Modeling thermal infrared (2 – 14 μm) reflectance spectra of frost and snow, *J. Geophys. Res.*, *99,* 24,241-24250.

Wan, Z., Y. Zhang, Q. Zhang, Z-L Li (2002), Validation of the land-surface temperature products retrieved from Terra Moderate Resolution Imaging Spectroradiometer data, *Rem. Sens. Environ., 83,* 163-180.

Wan, Z. (2008), New refinements and validation of the MODIS land-surface temperature/emissivity products, *Rem. Sens. Environ.*, *112,* 59-74.

Wang, X. and J. Key (2003), Recent trends in Arctic surface, cloud, and radiation properties from space, *Science*, *299*(5613), 1725-1728.

Wang, X. and J. Key (2005), Arctic surface, cloud, and radiation properties based on the AVHRR Polar Pathfinder data set. Part II: Recent trends, *Jour. Clim.*, *18*(14), 2575-2593.

940

941 Wang, L., M. Sharp, B. Rivard, and K. Steffen (2007), Melt season duration and ice layer
942 formation on the Greenland ice sheet, 2000-2004, *J. Geophys. Res.*, *112*, F04013,
943 doi:10.1029/2007JF000760.

944

945 Wismann, V. (2000), Monitoring of seasonal snowmelt on Greenland with ERS
946 Scatterometer data, *IEEE Trans. Geosci. Rem. Sens., 38*(4), 1821-1826.

947

948 Zwally, H.J., M.B. Giovinetto, J.Li, H.G. Cornejo, M.A. Beckley, A.C. Brenner, J.L.
949 Saba and D. Yi (2005), Mass changes of the Greenland and Antarctic ice sheets and
950 shelves and contributions to sea-level rise: 1992–2002, *Jour. Glaciol., 51*(175),509-527.

951

952 Figures

953

954 Figure 1a & b. Maps developed from blending MODIS land-surface temperature (LST)
955 and QuikSCAT (QS) melt maps from: 1a. 1 June 2007; and 1b. 2 June 2007. Note the
956 melt along the eastern and western margins of the ice sheet.

957

958 Figure 2a, b, c & d. 2a. MOD10A1 albedo map from 3 June 2007 illustrating pronounced
959 reduced albedo in the western margin of the Greenland Ice Sheet corresponding with
960 surface melt; 2b. 3 June 2007 land-surface temperature (LST) – QuikSCAT (QS)
961 blended map; the locations of transects in 2c (east) & d (southwest) are shown as the
962 black lines in Figures 2a & b. The locations shown on the vertical axes represent number
963 of kilometers from the start of the transect; note that the horizontal scale is different in
964 Figures 2c and 2d. The MODIS LST and albedo maps, though acquired on the same day,
965 often show different areas of cloud obscuration because the algorithms to produce each
966 daily product may each select different swaths (from different times of the day) and
967 clouds may thus be in different places. Dashed line is elevation; solid line is albedo.

968

969 Figure 3a, b, c & d. 3a. Extensive area of melt in southern Greenland as detected by the
970 MOD10A1 albedo product on 5 July 2007; 3b. MODIS land-surface temperature (LST)
971 – QuikSCAT (QS) blended map from 5 July 2007; 3c. Transect showing albedos and
972 delineation of melt zones from an area in 3c. The locations of transects in Figures 3c &
973 d are shown as the black line in Figures 3a (east) & b (southwest). (White areas in Figure
974 3d indicate areas where the albedo was <20% or missing.) The MODIS LST and albedo

975 maps, though acquired on the same day, often show different areas of cloud obscuration
976 because the algorithms to produce each daily product may each select different swaths
977 (from different times of the day) and clouds may thus be in different places. Dashed line
978 is elevation; solid line is albedo.
979
980
981 Figure 4a, b & c. 4a. MOD10 albedo map from 4 August 2007 showing reduced albedo
982 in refrozen snow area of the southern part of the ice sheet; 4b. MODIS land-surface
983 temperature (LST) – QuikSCAT (QS) blended map from 4 August 2007 showing that
984 nearly all of the ice sheet in southern Greenland has refrozen; 4c. Transect in southern
985 Greenland. The location of the transect in Figure 4c is shown as the black line in Figures
986 4a & b. The MODIS LST and albedo maps, though acquired on the same day, often
987 show different areas of cloud obscuration because the algorithms to produce each daily
988 product may each select different swaths (from different times of the day) and clouds
989 may thus be in different places. Dashed line is elevation; solid line is albedo.
990
991
992 Figure 5a, b & c. 5a. MOD10A1 albedo map from 13 August 2007 showing reduced
993 albedo in refrozen snow area in the southern part of the ice sheet; 5b. MODIS land-
994 surface temperature (LST) – QuikSCAT (QS) blended map from 13 August 2007
995 showing active melt in southern Greenland; 5c. The location of the transect across the ice
996 sheet is shown in Figures 5a & b. The MODIS LST and albedo maps, though acquired
997 on the same day, often show different areas of cloud obscuration because the algorithms

998 to produce each daily product may each select different swaths (from different times of
999 the day) and clouds may thus be in different places. Dashed line is elevation; solid line is
1000 albedo.
1001
1002 Figure 6. MOD10A1 albedo plots from 12 and 13 August 2007 showing lowering of
1003 albedo from 12 to 13 August where extensive melt on 13 August has caused the albedo to
1004 decrease due to grain size increases.
1005
1006 Figure 7a & b. 7a. Minimum albedo on a per-pixel basis as determined from the MODIS
1007 daily snow albedo product, MOD10A1. 7b. Total extent of seasonal snow melt from the
1008 MODIS land-surface temperature (LST) and QuikSCAT (QS) melt maps.

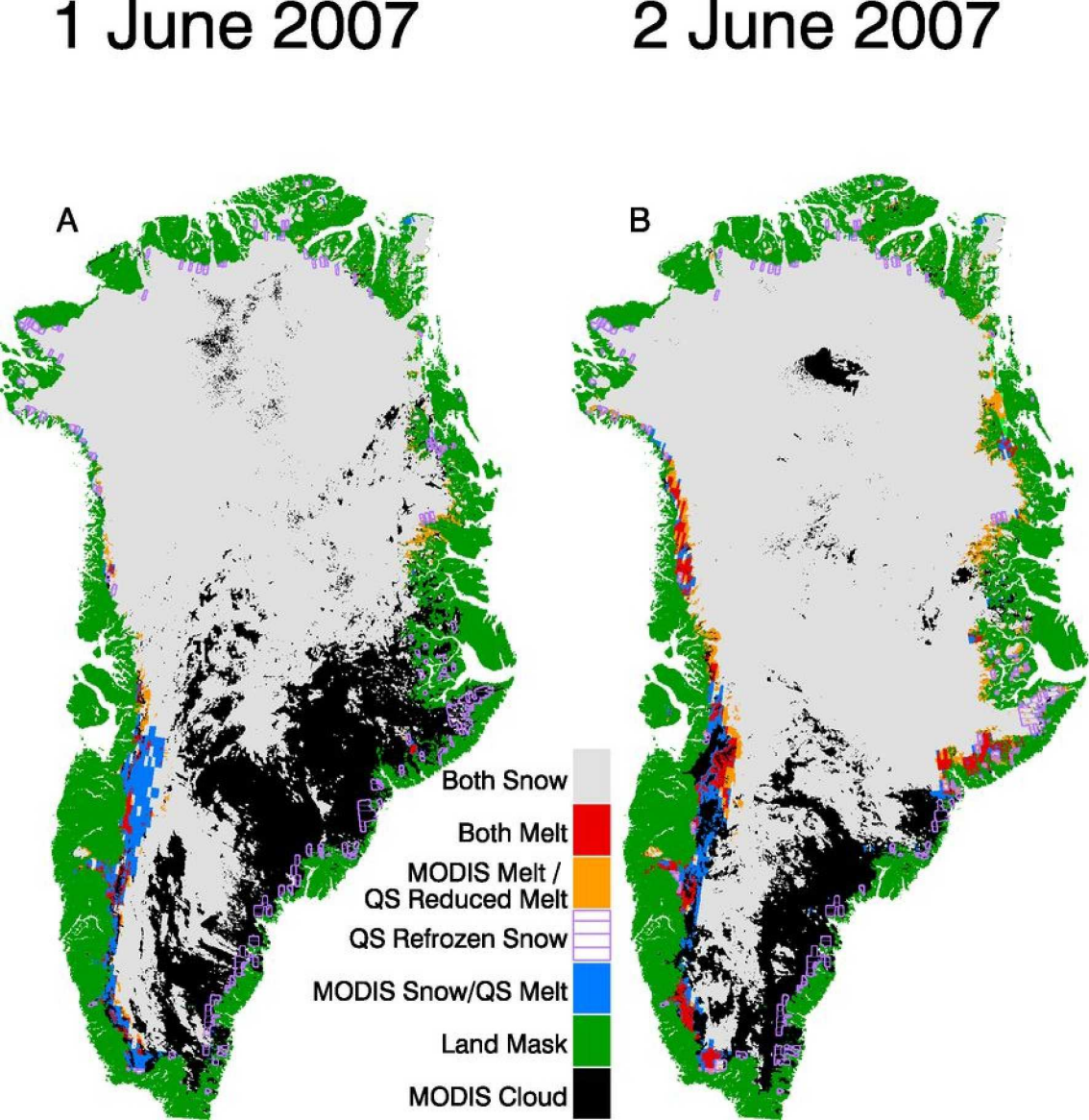
1 June 2007
2 June 2007
A
B
Both Snow
Both Melt
MODIS Melt /
QS Reduced Melt
QS Refrozen Snow
MODIS Snow/QS Melt
Land Mask
MODIS Cloud

3 June 2007

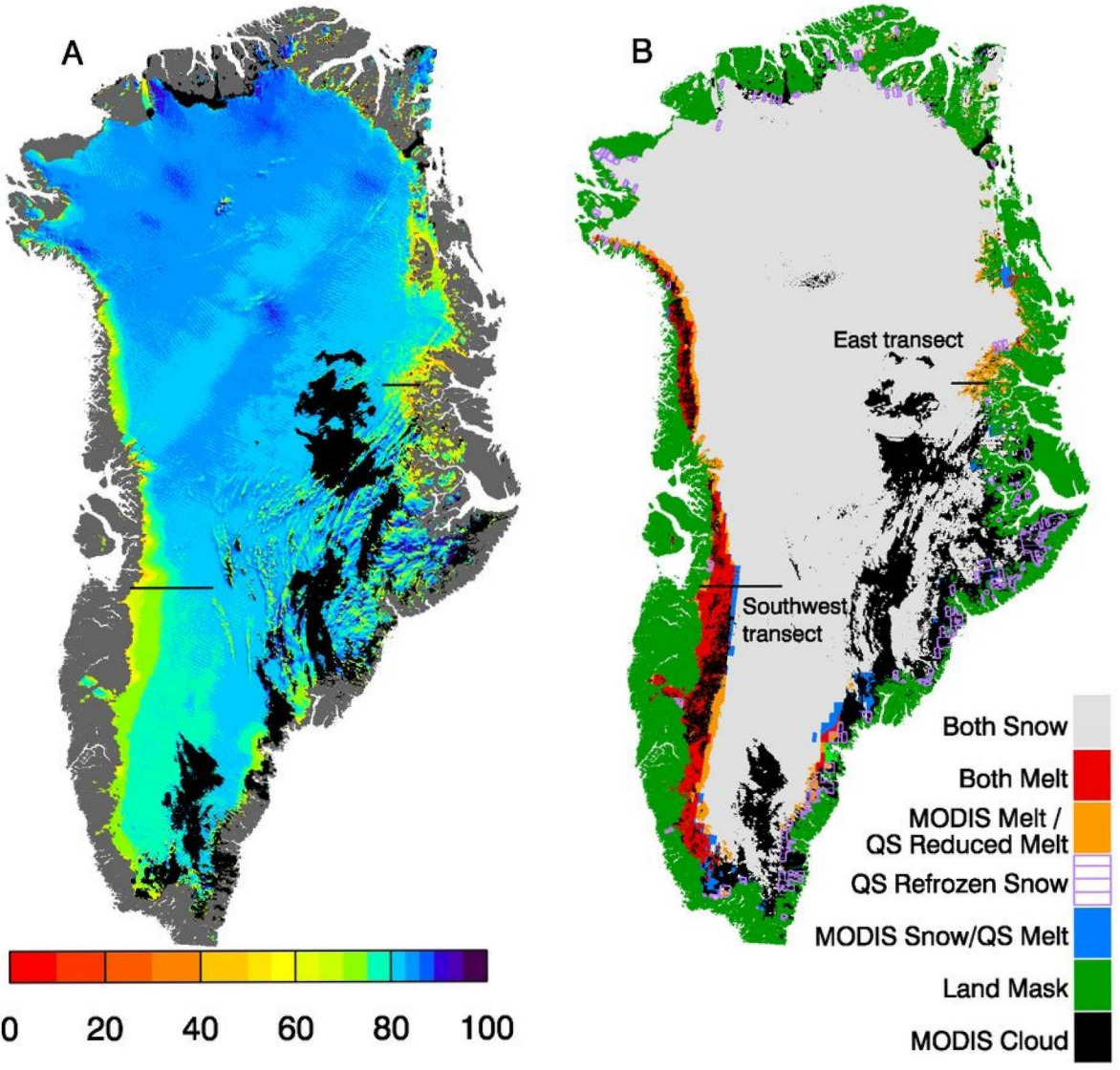
A
B
East transect
Southwest transect
Both Snow
Both Melt
MODIS Melt / QS Reduced Melt
QS Refrozen Snow
MODIS Snow/QS Melt
Land Mask
MODIS Cloud
0
20
40
60
80
100

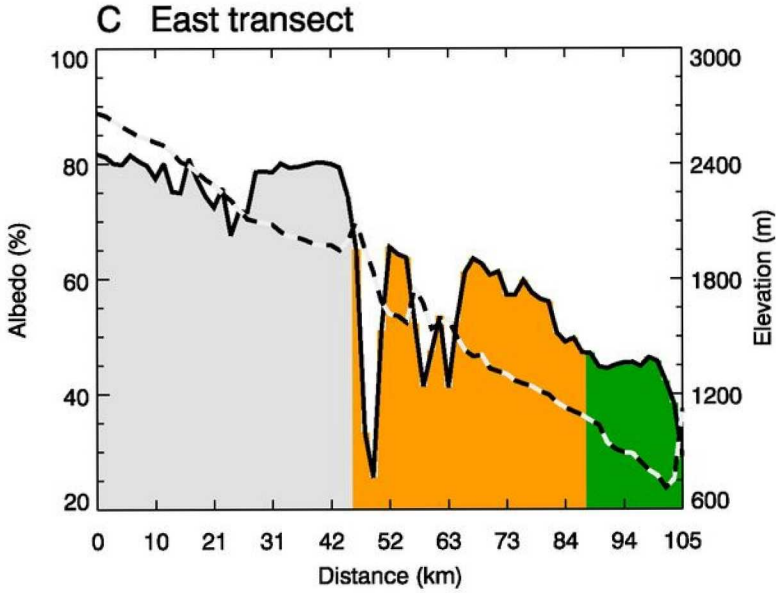
C East transect
Albedo (%)
Elevation (m)
Distance (km)
100
80
60
40
20
3000
2400
1800
1200
600
0
10
21
31
42
52
63
73
84
94
105

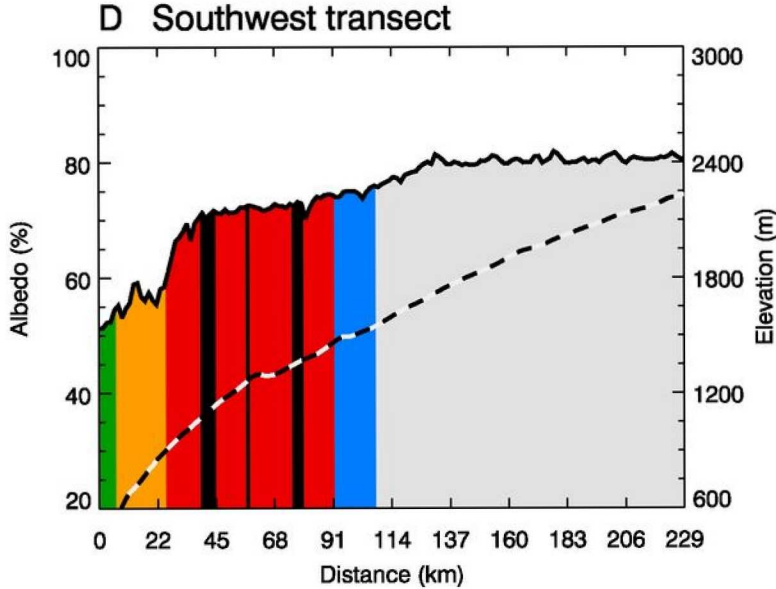
D Southwest transect
Albedo (%)
Elevation (m)
Distance (km)
100
80
60
40
20
3000
2400
1800
1200
600
0
22
45
68
91
114
137
160
183
206
229

5 July 2007

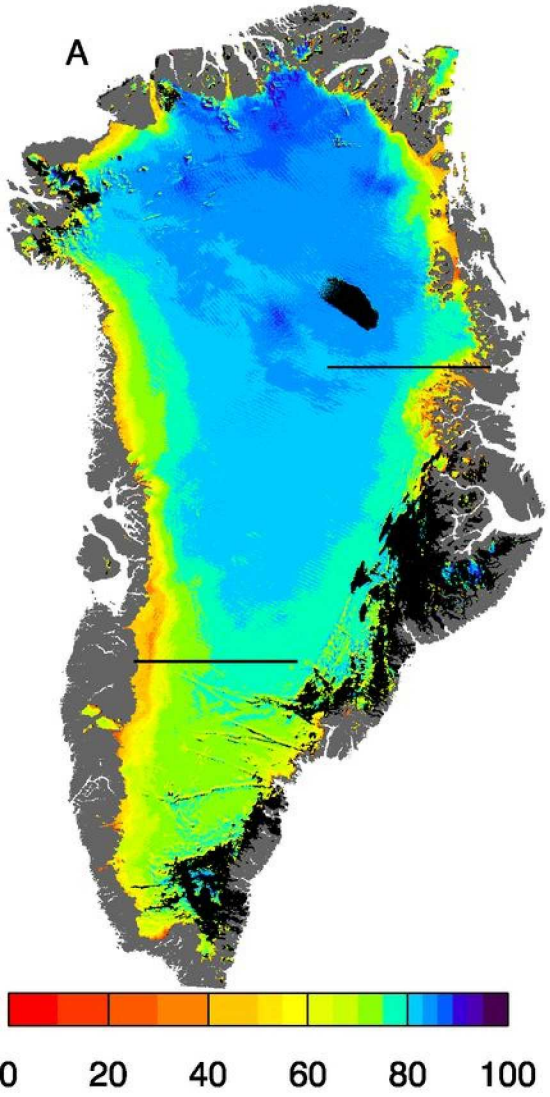
A
0
20
40
60
80
100

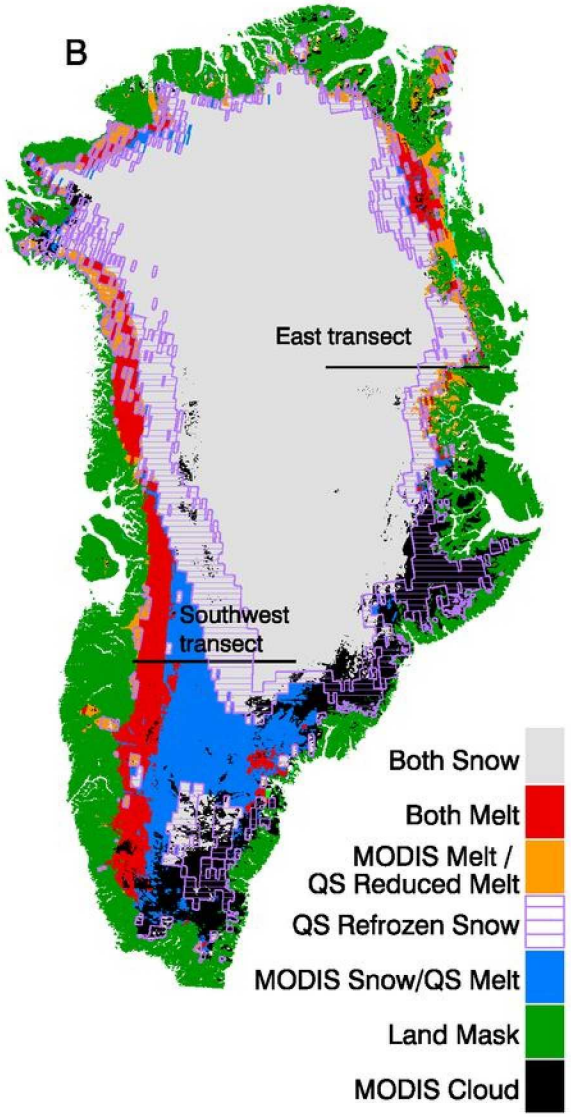
B
East transect
Southwest transect
Both Snow
Both Melt
MODIS Melt / QS Reduced Melt
QS Refrozen Snow
MODIS Snow/QS Melt
Land Mask
MODIS Cloud

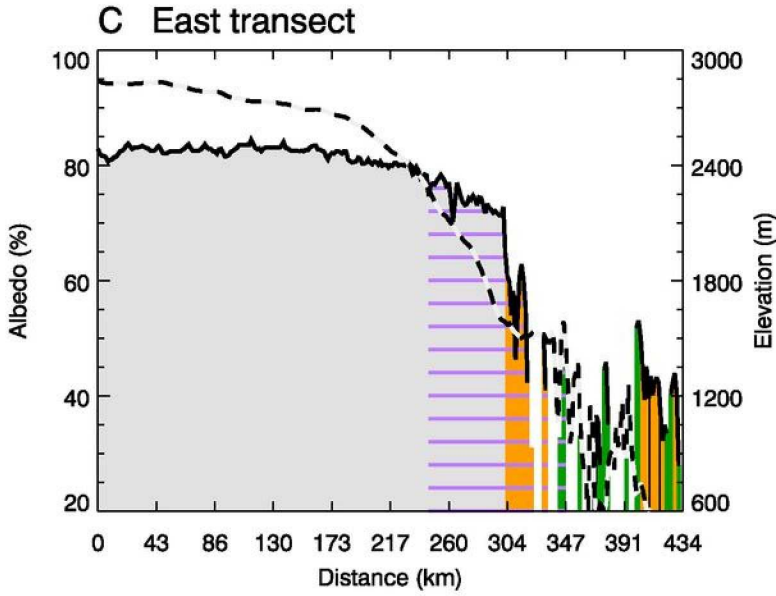
C East transect
Albedo (%)
Elevation (m)
100
80
60
40
20
3000
2400
1800
1200
600
0 43 86 130 173 217 260 304 347 391 434
Distance (km)

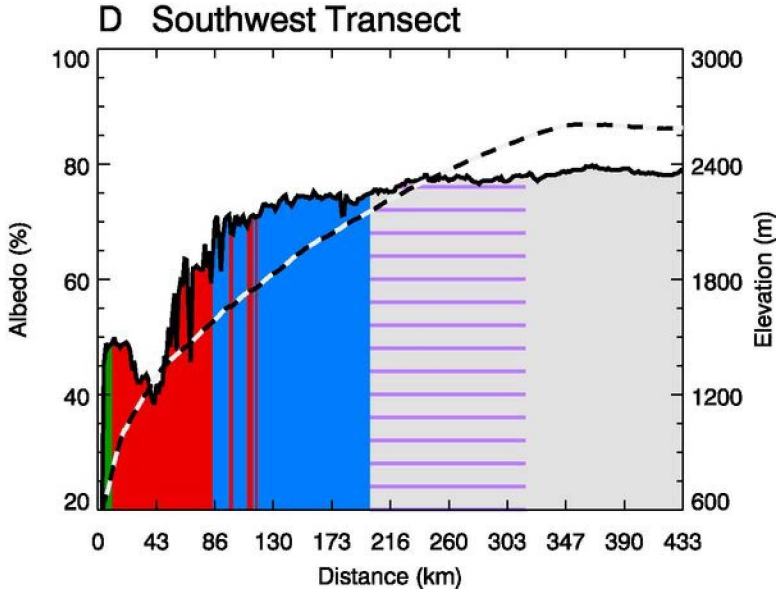
D Southwest Transect
Albedo (%)
Elevation (m)
100
80
60
40
20
3000
2400
1800
1200
600
0 43 86 130 173 216 260 303 347 390 433
Distance (km)

4 August 2007

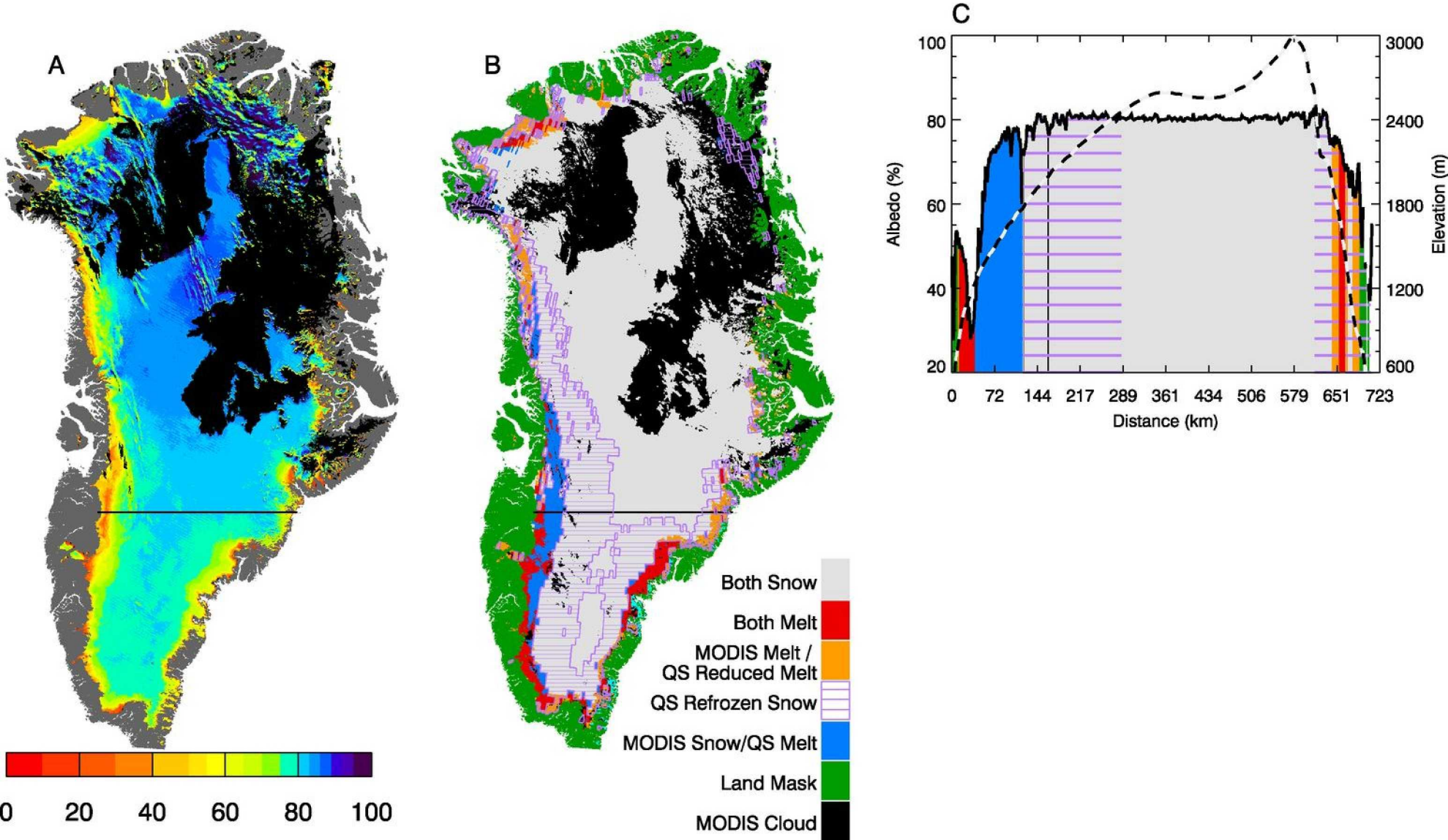

13 August 2007

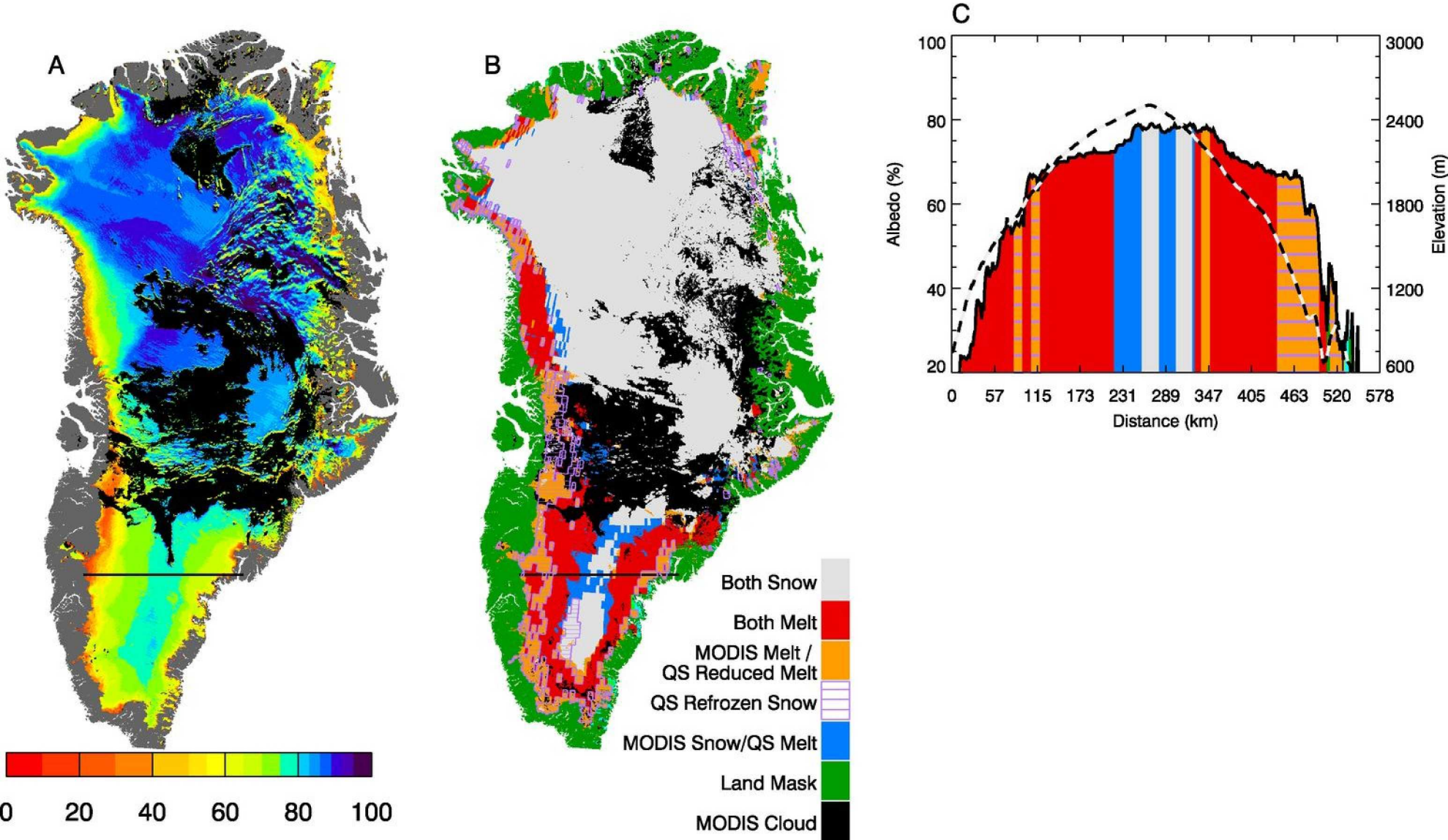

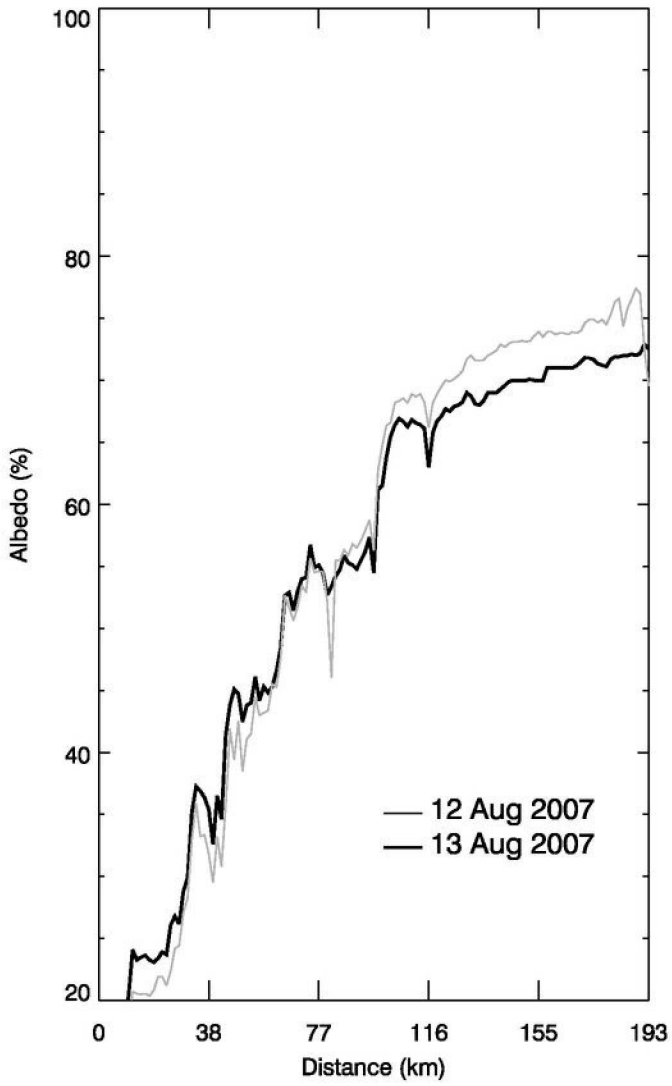
100
80
60
40
20
Albedo (%)
0
38
77
116
155
193
Distance (km)
12 Aug 2007
13 Aug 2007

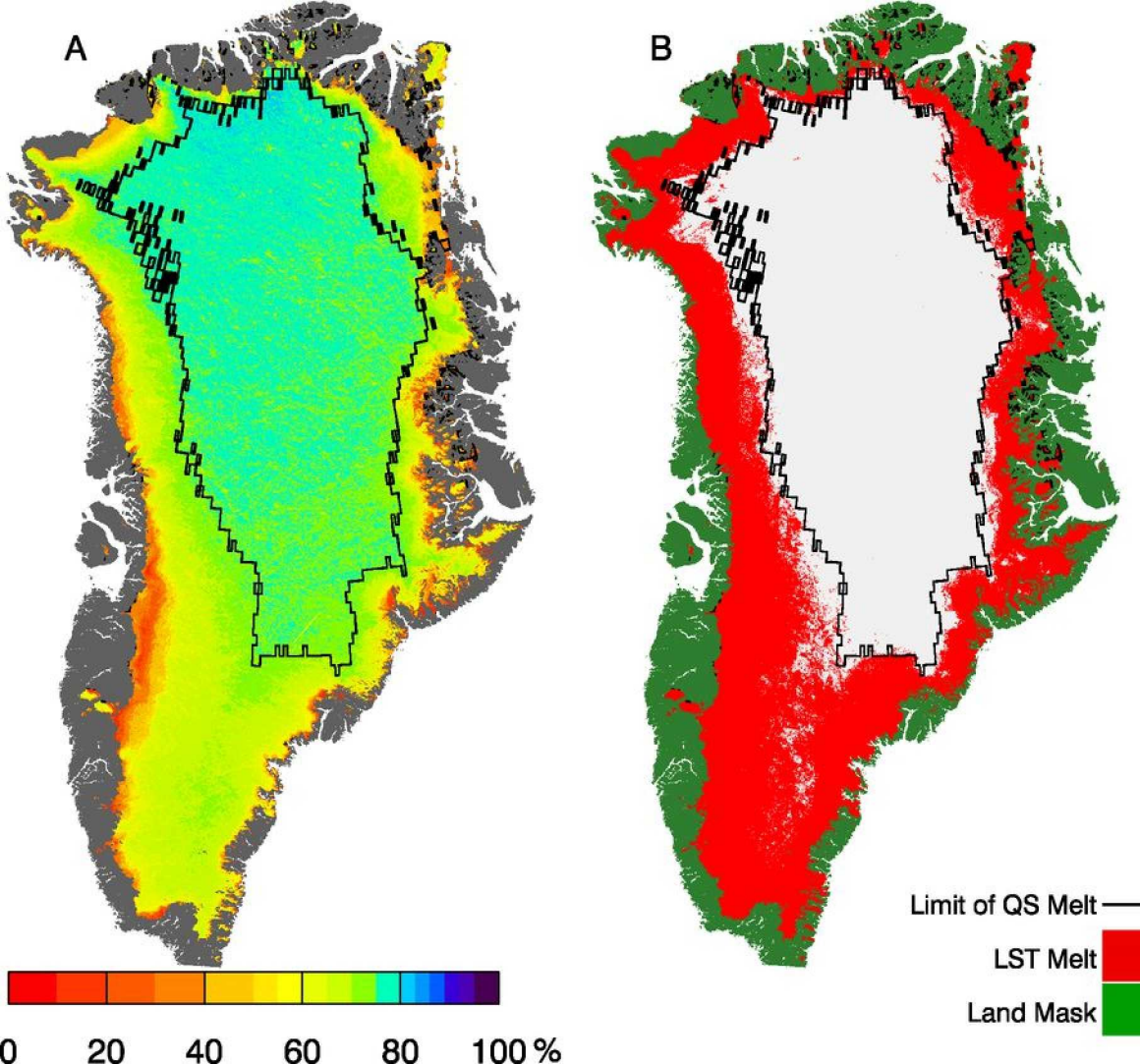
A
B
0
20
40
60
80
100 %
Limit of QS Melt
LST Melt
Land Mask